Aspiration of Human Neutrophils: Effects of Shear Thinning and Cortical Dissipation

Jeanie L. Drury and Micah Dembo
Boston University, Department of Biomedical Engineering, Boston, Massachusetts 02215, USA

ABSTRACT It is generally accepted that the human neutrophil can be mechanically represented as a droplet of polymeric fluid enclosed by some sort of thin slippery viscoelastic cortex. Many questions remain however about the detailed rheology and chemistry of the interior fluid and the cortex. To address these quantitative issues, we have used a finite element method to simulate the dynamics of neutrophils during micropipet aspiration using various plausible assumptions. The results were then systematically compared with aspiration experiments conducted at eight different combinations of pipet size and pressure. Models in which the cytoplasm was represented by a simple Newtonian fluid (i.e., models without shear thinning) were grossly incapable of accounting for the effects of pressure on the general time scale of neutrophil aspiration. Likewise, models in which the cortex was purely elastic (i.e., models without surface viscosity) were unable to explain the effects of pipet size on the general aspiration rate. Such models also failed to explain the rapid acceleration of the aspiration rate during the final phase of aspiration nor could they account for the geometry of the neutrophil during various phases of aspiration. Thus, our results indicate that a minimal mechanical model of the neutrophil needs to incorporate both shear thinning and surface viscosity to remain valid over a reasonable range of conditions. At low shear rates, the surface dilatation viscosity of the neutrophil was found to be on the order of 100 poise-cm, whereas the viscosity of the interior cytoplasm was on the order of 1000 poise. Both the surface viscosity and the interior viscosity seem to decrease in a similar fashion when the shear rate exceeds $\sim 0.05\ s^{-1}$. Unfortunately, even models with both surface viscosity and shear thinning studied are still not sufficient to fully explain all the features of neutrophil aspiration. In particular, the very high rate of aspiration during the initial moments after ramping of pressure remains mysterious.

INTRODUCTION

Neutrophils function primarily to phagocytize microbial pathogens (bacteria, yeast, etc.) and to remove dead cells and necrotic tissues. To accomplish these tasks, the cells need a large cytoplasmic volume, and, as a result, their diameter, 9 μm, is about twice that of a typical capillary vessel (Ting-Beall et al., 1993). Remarkably, despite this size mismatch, neutrophils are passively carried with the circulating blood to all regions of the body, and instances where they plug the capillaries are exceedingly rare. The mechanical adaptations that support this normal circulation and the pathologies that result from failures of these adaptations have been studied experimentally primarily via micropipet aspiration, because this technique is uniquely capable of reproducing the physiological deformations and stresses encountered during capillary transit.

Early aspiration experiments indicated that the cytoplasm of human neutrophils behaved like a highly viscous fluid with very little elasticity (Evans and Kukan, 1984; Evans and Yeung, 1989; Needham and Hochmuth, 1990). It was also discovered that neutrophils have a static cortical tension (Evans and Yeung, 1989; Needham and Hochmuth, 1992; Albarran et al., 2000), that they enter the pipet in an isovolumetric manner, and that they slip freely over the pipet walls with little tendency to adhere (Needham and Hochmuth, 1990; Shao and Hochmuth, 1997). Finally, it was demonstrated that the increase in apparent surface area during aspiration is accommodated purely by a smoothing of microscopic folds and wrinkles of the plasma membrane and that the total area of plasma membrane remains unchanged (Schmid-Schönbein et al., 1980; Evans and Yeung, 1989). Thus, from a mechanical point of view, the neutrophil can be regarded as consisting of a fluid core enclosed in some kind of thin slippery viscoelastic surface layer.

Despite this clarity on the general level, there is still uncertainly about the more detailed aspects of the so called "slippery droplet model." For example, some studies suggest a significant surface viscosity of the cortex (Yeung and Evans 1989; Evans and Yeung 1989) whereas other data suggest that the viscosity of the cortex is actually lower than the viscosity of the interior cytoplasm (Dong and Skalak, 1992). In yet another study, (Tsai et al., 1993), a decrease in the apparent viscosity of the cytoplasm was reported when experiments were conducted at high aspiration pressures. This was interpreted as indicating shear thinning of the cytoplasm, whereas other studies have indicated a Newtonian cytoplasm (Evans and Yeung 1989). Still other reports have suggested that the bulk cytoplasm is capable of storing significant elastic energy (Schmid-Schönbein et al., 1981; Sung et al., 1988; Dong et al., 1988, 1991; Lipowsky et al., 1991; Dong and Skalak, 1992).

In the present work, we use large scale finite element calculations to analyze several hypothetical versions of the slippery droplet model and to determine which notions

Received for publication 27 July 2000 and in final form 7 August 2001.

Address reprint requests to Micah Dembo, Boston University, Dept. of Biomedical Engineering, 44 Cummington Street, Boston, MA 02215-2407. Tel.: 617-353-1671; Fax: 617-353-6766; E-mail: mxd@bu.edu.

0006-3495/01/12/3166/12 $2.00

TABLE 1 Experimental conditions

Experiment	ΔP (dynes/cm^2)	R_p (μm)	Number of cells	$\dot{L}_{p50} \pm$ SD (μm/s)
1	470	2.2	4	0.0277 ± 0.0074
2	687	2.2	5	0.0570 ± 0.025
3	1430	2.2	6	0.137 ± 0.024
4	3172	2.2	11	0.702 ± 0.24
5	14204	2.2	24	9.173 ± 4.70
6	164	3.2	4	0.109 ± 0.014
7	1346	3.2	30	2.023 ± 1.08
8	5124	3.2	21	22.37 ± 12.02

ΔP, average applied pressure; R_p, pipet radius; and $\dot{L}_{p50} \pm$ SD, average rate of entry at the point where the cell is 50% aspirated plus or minus the standard deviation.

about the detailed mechanical properties of the interior fluid and the cortex are in best agreement with observed neutrophil aspiration dynamics. Specifically, we explore the consequences of cortical dissipation and of shear thinning and of various notions about the behavior of the plasma membrane.

METHODS

Experimental measurements and data processing

Measurements of cell aspiration were conducted under eight combinations of pipet size and aspiration pressure as summarized in Table 1. The basic system for micropipet aspiration was similar to that used previously by Evans and Yeung (1989). In all experiments, cells were obtained from a single donor via a finger prick and suspended in Heinz Hepes Buffer with 1 gm% bovine albumin. The micropipets were pulled with a vertical pipet puller (Model 700C, David Kopf Instruments, Tujunga, CA) and chosen such that their internal diameter was between 4 and 6.5 μm. Cells selected for study were initially held at a very low pressure (~1 dyne/cm^2) so that they could be examined and characterized. A cell was rejected at this stage if there was evidence of activation (protrusions, asymmetry, or stickiness) or if the diameter was larger than 9 μm or less than 8.5 μm. Following the initial characterization, the suction pressure in the pipet was suddenly ramped at a rate of 100,000 dynes/cm^2/s, to the desired final value with a Harvard Apparatus PHD 2000 syringe pump (Holliston, MA) coupled with a continuous manometer system (transducers by Validyne, Northridge, CA). The ramping rate and final pressure were computer controlled and the zero of time was taken at the midpoint of the ramp. Overall, experiments were completed within 40 minutes of the finger prick. After this time, the cells were discarded and a new sample was prepared. In a few cases, cells became activated or started to adhere to the pipet subsequent to the start of aspiration. Because such cells did not complete aspiration, these data were discarded.

Hoffman modulation contrast (Hoffman and Gross, 1975; http://micro.magnet.fsu.edu/primer/techniques/hoffman.html, 2000) was used to visualize the cells. A CCD72 video camera (DAGE-MTI, Michigan City, IN) was used to capture the Hoffman contrast image of the cell and pipet. This image was then displayed on a monitor and recorded on video tape. A line marker (three video lines wide) was positioned along the center of the long axis of the pipet, and an intensity profile along this marker was collected every 1/30 s. These intensity values were then added to obtain a single intensity profile along the center axis of the pipet and the aspirating cell. Fringes in this intensity profile were used to determine the position of the leading and trailing edges of the cell and the position of the pipet nozzle.

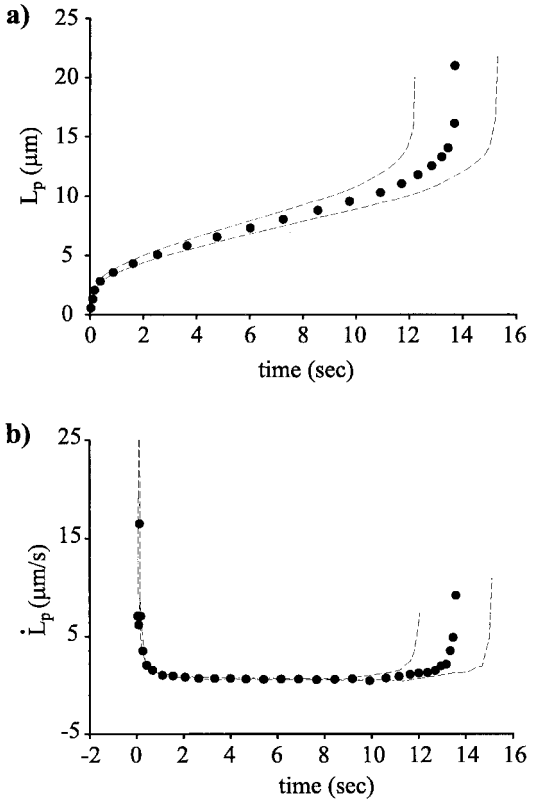

FIGURE 1 The typical kinetics of neutrophil aspiration. Eleven different cells were aspirated under the conditions of Exp. 4 of Table 1 ($R_p = 2.2$ μm and $\Delta P = 3172$ dynes/cm^2). Data from all cells were then combined and the average time required to reach various preset values of L_p was determined. (*a*) L_p versus $\bar{t}(L_p)$ (*closed circles*) and also the ±SEM envelope (*dashed lines*). (*b*) Corresponding graph of the time derivative $\dot{L}_p$.

Several standard quantities provided observable scalar measures of droplet shape and of the extent and progress of aspiration (Drury and Dembo, 1999). The extent of cell aspiration was mainly characterized in terms of the axial distance separating the opening of the pipet and the most aspirated pole of the cell, $L_p(t)$. The external geometry of the cell was characterized in terms of a cylindrical coordinate system (r, θ, z) by defining $R_{max}(t)$ as the radius of the cell at the widest point and $Z_{min}(t)$ as the minimum value of the axial coordinate. Other useful quantities associated with aspiration were the volume of cytoplasm contained within the lumen of the pipet, $V_{asp}(t)$ and the projected (or apparent) surface area of the cell, A. The rate of droplet aspiration was described in terms of time derivatives (i.e., $\dot{Q} = \partial_t V_{asp}(t)$, $\dot{A} = \partial_t A(t)$, and $\dot{L}_p \equiv \partial_t L_p(t)$).

For each experimental condition listed in Table 1, the data for all cells were combined to determine $\bar{t}(L_p)$, (the time required for an average cell to reach a given value of L_p). Figure 1 *a* shows a plot of L_p against $\bar{t}(L_p)$ for a typical experiment, and Fig. 1 *b* shows the associated plot of $\dot{L}_p$. As seen in these results, the dynamical process by which the neutrophil enters a micropipet is roughly divisible into three temporal phases. Immediately after ramping the aspiration pressure, the cell "jumps" into the opening of the pipet at a rapidly decelerating rate (thus $\ddot{L}_p$ is large in a negative sense). Subsequently, $\dot{L}_p$ stabilizes and remains approximately constant for an extended period (thus $\ddot{L}_p \approx 0$). Last, $\ddot{L}_p$ becomes positive and $\dot{L}_p$ increases toward an infinite value just as the cell disappears into the interior of the pipet. These three phases, the initial jump, the intermediate linear phase, and the final jump, can be discerned, to various degrees, for all different choices of the pipet radius and aspiration pressure. For each experimental

condition, the final column in Table 1 gives the population mean (±SD) of $\dot{L}_p$ at the point where ~50% of the cell volume had been aspirated (denoted by $\dot{L}_{p50}$). The ratio $\bar{s} \equiv \dot{L}_{p50}/R_p$ provides a useful empirical measure of the average shear rate of the cytoplasmic flow field at each experimental condition.

Our subsequent analysis is based on the common-sense idea that population-averaged aspiration curves of the sort shown in Fig. 1 *a* are equivalent to multiple experiments carried out on a single cell of average properties. According to this philosophy, a mechanical model of the neutrophil should be able to account for our aspiration data, over the complete range of pipet diameters and aspiration pressures, with a single choice for any and all invoked material moduli. In fact, this is a utilitarian viewpoint because it is difficult to see what use there could be for a model that failed such a test. In the present circumstances, the existence of a model of the neutrophil satisfying this minimum utilitarian property is supported by the rather modest degree of cell-to-cell variation observed. Indeed, at low aspiration pressures, the aspiration curves for different cells were virtually identical so that good statistics could be obtained with only a few replicates. At higher pressures, cell-to-cell dispersion became significant, and it was necessary to increase the number of experiments to obtain reasonable error limits on the average behavior. In all cases, however, the dispersion of the data was well represented by a Gaussian with no extreme outliers. Furthermore, there were always several cells that followed very closely to the population average.

Continuum description of the neutrophil

Our theoretical approach to the mechanics of the neutrophil aspiration is a generalization of an earlier analysis that was restricted to the case of Newtonian cytoplasm and constant surface tension (Drury and Dembo, 1999). Briefly, cylindrical coordinates (r, θ, z) are introduced and used to define the pipet (a cylindrical cavity drilled into the half space, $z > 0$, with interior radius, R_p) and the cell (a slippery and incompressible droplet of fluid occupying a simply connected region, $\Omega(t)$). At $t = 0$, the region $\Omega(t)$ is a sphere of radius, R_c (see Fig. 2 *a*). Within Ω, the velocity and pressure of the cytoplasm are assumed to satisfy the Stokes equations

$$\nabla \cdot \mathbf{v} = 0 \tag{1a}$$

and

$$\nabla \cdot (\mu(\nabla \mathbf{v} + (\nabla \mathbf{v})^{\mathrm{T}}) - p\mathbf{I}) = 0. \tag{1b}$$

Here, p and $\mathbf{v}$ are the pressure and velocity fields, μ is the coefficient of viscosity, and $\mathbf{I}$ is a unit tensor.

Conceptually, the cohesion of a complex polymer network can vary from point to point because local shearing motions tend to decrease the density of rheologically important microfeatures (e.g., cross-links and entanglements). Upon cessation of shearing, diffusion and cross-linking reactions then restore the equilibrium distribution of these features. A well-known approach to representing such physics (Bird et al., 1960) involves letting the coefficient of viscosity vary as a monotone-decreasing point function of a certain invariant scalar called the shear rate,

$$s \equiv \sqrt{0.5((\nabla \mathbf{v} + (\nabla \mathbf{v})^{\mathrm{T}}) : (\nabla \mathbf{v} + (\nabla \mathbf{v})^{\mathrm{T}}))}\,. \tag{2a}$$

The detailed functional dependency of μ on s is open to argument, but, for our current purpose, it will be sufficient to adopt an empirical form,

$$\mu = \mu_0 \left(1 + \frac{s}{s_c}\right)^{-b}, \tag{2b}$$

which yields a kind of generalized power law fluid. The material constants, μ_0, s_c, and b, are the low-shear bulk viscosity, the characteristic shear rate, and the shear thinning exponent, respectively. Note that this shear thinning fluid reduces to a Newtonian fluid with a viscosity, μ_0 if $s/s_c \ll 1$ or if the exponent, $b \to 0$.

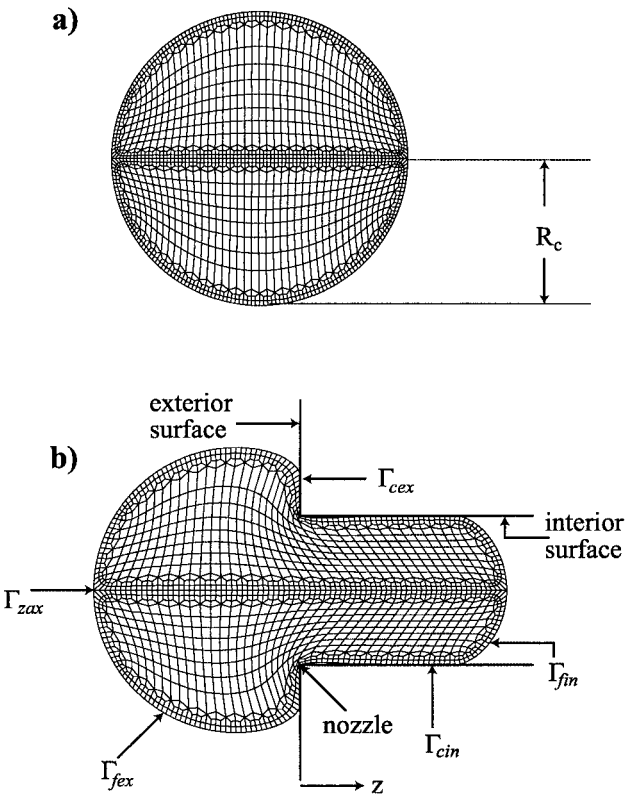

FIGURE 2 Geometry of a typical computational domain at two stages. (*a*) The domain in its initial, round state. (*b*) The domain has been partially aspirated into the pipet. Here, the interior, exterior, and nozzle of the pipet are indicated. Γ_{fin}, free-interior; Γ_{fex}, free-exterior; Γ_{cin}, constrained-interior; and Γ_{cex}, constrained-exterior boundaries. There is a fifth, purely logical boundary, Γ_{zax}, which is the axis of symmetry.

Turning now to the surface of the neutrophil, we confront the problem of representing the very fine geometry of the wrinkles and folds that characterize the plasma membrane. Because it is impractical to fully resolve these fine structures, we attempt to represent the neutrophil geometry only to resolution of the light microscope. A special surface density field, ρ, is then introduced as a measure of the amount of the unresolved or excess area of the plasma membrane at various surface locations (ρ defined as the cm^2 of actual membrane bilayer per cm^2 of "resolved" area). When the resolved surface is spherical, ρ takes the constant value of $\rho_0 \approx 2.1$ in accord with well-established experimental results (Evans and Yeung, 1989). A value of $\rho = 1$ implies that the resolved area and the actual area are identical. As aspiration goes forward, the excess area is transported laterally via the surface flow and may also increase or decrease as the resolved surface expands and contracts. All of these possibilities are properly taken into account by allowing ρ to evolve according to the transport equation,

$$d_t\rho = \nabla_s \cdot (D_m \nabla_s \rho) - \rho \nabla_s \cdot \mathbf{v}. \tag{3}$$

Here, d_t is the substantial derivative for an observer moving with the cytoplasmic velocity at an arbitrary surface location and ∇_s and $\nabla_s \cdot$ are the surface gradient and surface divergence, respectively. Thus, $\nabla_s \cdot (D_m \nabla_s \rho)$ is a surface diffusion term that results for slippage of the membrane over the cytoplasm, and $\nabla_s \cdot \mathbf{v}$ is the rate of surface dilation. Appendix A provides a derivation and explanation of Eq. 3 with particular emphasis on

the origin of the so-called "wrinkle diffusion" term. In the subsequent discussion, we will need to consider two important limiting cases of Eq. 3: strong membrane–cytoplasmic coupling ($D_m \to 0$) and weak membrane–cytoplasmic coupling ($D_m \to \infty$). In the latter limit, the amount of wrinkling is essentially uniform over the entire surface but changes with time because the resolved mesh area increases as aspiration proceeds.

The interaction of the droplet with the pipet means that the resolved boundary of $\Omega(t)$ is generally comprised of several submanifolds Γ_{fin}, Γ_{cin}, Γ_{cex}, and Γ_{fex}. These are the free-interior, constrained-interior, constrained-exterior, and free-exterior surfaces, respectively (see Fig. 2 *b*). All of these manifolds are able to grow or shrink in extent and shape as functions of time, and in some configurations, certain manifolds (e.g., Γ_{cex}) did not exist at all. Considering only isotropic surface stresses, the boundary conditions for Stokes's equations on the various manifolds can be stated as (see Aris 1989 for derivation)

$$(\mu(\nabla\mathbf{v} + (\nabla\mathbf{v})^T) - p\mathbf{I})\cdot\mathbf{n} = [-2\mathbf{n}\kappa + \nabla_s][\gamma + \eta\nabla_s\cdot\mathbf{v}] - P_{in}\mathbf{n} \quad \text{On } \Gamma_{fin}, \quad (4a)$$

$$(\mu(\nabla\mathbf{v} + (\nabla\mathbf{v})^T) - p\mathbf{I})\cdot\mathbf{n} = [-2\mathbf{n}\kappa + \nabla_s][\gamma + \eta\nabla_s\cdot\mathbf{v}] - P_{ex}\mathbf{n} \quad \text{On } \Gamma_{fex}, \quad (4b)$$

$$\mathbf{t}\cdot(\mu(\nabla\mathbf{v} + (\nabla\mathbf{v})^T))\cdot\mathbf{n} = \mathbf{t}\cdot(\nabla_s\gamma + \nabla_s(\eta\nabla_s\cdot\mathbf{v})), \quad \mathbf{v}\cdot\mathbf{n} = 0 \quad \text{On } \Gamma_{cin}, \quad (4c)$$

and

$$\mathbf{t}\cdot(\mu(\nabla\mathbf{v} + (\nabla\mathbf{v})^T))\cdot\mathbf{n} = \mathbf{t}\cdot(\nabla_s\gamma + \nabla_s(\eta\nabla_s\cdot\mathbf{v})), \quad \mathbf{v}\cdot\mathbf{n} = 0 \quad \text{On } \Gamma_{cex}. \quad (4d)$$

Here, $\mathbf{n}$ and $\mathbf{t}$ denote unit normal and tangent vectors of the boundary and κ is its mean curvature, ($\mathbf{n}$ points in the outward direction and $\mathbf{t}$ in the direction of increasing latitude, the sign of κ is taken to be positive when the center of curvature lies inside the cell). The surface fields γ and η are the surface tension and surface dilatation viscosities, respectively. These are defined on each of the boundary segments as continuous functions according to constitutive laws described below. Finally, P_{in} is the hydrostatic pressure acting inside the lumen of the pipet, and P_{ex} is the atmospheric pressure acting outside the pipet. Note that $P_{in} = P_{ex} - \Delta P$ where ΔP (the aspiration pressure) is determined from a manometer reading.

Detailed experimental measurements of neutrophils under various conditions of static deformation have established that the surface tension of a resting round cell falls in the narrow range $\gamma_0 \approx 0.024 - 0.035$ dynes/cm (Evans and Yeung, 1989; Needham and Hochmuth, 1992). The data also indicate a strong dependence of surface tension on the degree of membrane wrinkling. In particular, a 25% decrease in ρ results in a doubling of the apparent surface tension in typical cells (Needham and Hochmuth, 1992; Albarran et al., 2000). This connection of tension and excess area can be captured by a simple constitutive law of the form,

$$\gamma(\rho) = \gamma_0\left(\frac{\rho_0}{\rho}\right)^{\alpha}, \quad (5)$$

where the exponent α has a value quite close to 3.

Finally, the physical processes underlying shear thinning are expected to be similar in both the cortex and the bulk cytoplasm. We can therefore simplify matters by requiring that η should have the same shear rate dependence as μ. In view of Eq. 2b, this means that

$$\eta = \eta_0\left(1 + \frac{s}{s_c}\right)^{-b}, \quad (6)$$

where the values of s_c and b are as previously, and η_0 (units of poise·cm) is the limiting value of the dilatational surface viscosity when the shear rate is very low.

Numerical

Computational solutions of the governing equations just described were generated using a low Reynolds number hydrodynamics transport code based on the Galerkin finite element method. Details of this method have appeared elsewhere (Dembo, 1994a,b; He and Dembo, 1997; Drury and Dembo, 1999). In the case of calculations involving shear thinning, it was necessary to implement an iterative procedure at each time step to simultaneously solve for the velocity, shear rate, and viscosity. Exhaustive tests demonstrated that this iteration was globally convergent to a unique solution provided that the exponent of the shear thinning was less than 1. As a further control, the code was tested against analytic solutions for pipe flow of various power law fluids at different pressures and pipe sizes. In these tests, a mesh with spacing of ~3% of the pipe radius was sufficient to reproduce the expected analytic results to within 1% for values of $b \le 0.80$. For higher values of b, this mesh was unable to resolve the very sharp velocity gradients at the pipe wall, and performance deteriorated markedly.

RESULTS

Simple models with Newtonian cytoplasm

As a coupled system, Eqs. 1–6 invoke a total of nine parameters to fully describe the mechanics of a neutrophil (R_c, ρ_0, γ_0, α, μ_0, η_0, s_c, b, and D_m). Of these, the values of R_c, ρ_0, γ_0, and, α are well established (described in Methods section). The simplest interesting case of our general model (hereafter called M1) was then obtained by holding the known parameters at their established values by neglecting shear thinning (s_c, b) $\to$ (∞, 0) and surface dissipation $\eta_0 \to 0$ and by allowing free slip of the membrane with respect to the cytoplasm, $D_m \to \infty$ (weak membrane–cytoplasmic coupling). The remaining parameter of M1 (μ_0) was then derived by selecting two of the experiments in Table 1 and conducting numerical computations with various choices of this parameter until there was good agreement between the calculated and observed values of $\dot{L}_{p50}$ for these experiments (see Table 2 for a complete list of parameters and a description of the general features that distinguish each model).

Figure 3, *a–h*, shows our averaged aspiration data for the eight experimental conditions of Table 1 (*closed circles*) and the results of finite element computations for various models. The simplest way to analyze these results involves neglecting all subtle features of the data and focusing only on the general time scale of aspiration (this is more or less equivalent to comparison based only on predicted and observed $\dot{L}_{p50}$ values). Via this approach, the theoretical predictions of M1 (labeled "1" in Fig. 3) is seen to be in fair agreement with the data in Fig. 3, *a* and *b* (this was not surprising because these were the two experiments used for determining the value of μ_0). Under all other conditions, the model grossly underestimated the true time scale of aspiration. Moreover, the magnitude of this underestimation pro-

TABLE 2 Model parameters

Parameter	M†	M2	M3	M4	M5	M6
R_c (μm)*	4.25	4.25	4.25	4.25	4.25	4.25
μ_0 (poise)	6000	6000	6000	6000	1100	1100
η_0 (poise·cm)	0	0	0	0	100	100
γ_0 (dynes/cm)	0.03	0.03	0.03	0.03	0.03	0.03
α	3	3	3	3	3	3
ρ_0 (cm/cm)	2.1	2.1	2.1	2.1	2.1	2.1
D_m (cm^2/s)	∞	0	∞	0	0	0
s_c (1/s)	∞	∞	0.05	0.05	∞	0.05
b	0	0	0.5	0.5	0	0.5

*R_c, average cell radius; μ_0, low-shear bulk viscosity (Eq. 2b); η_0, low-shear dilatational surface viscosity (Eq. 6); γ_0, resting surface tension (Eq. 5); α, exponent of the surface tension constitutive law (Eq. 5); ρ_0, is the initial excess area density; D_m, excess area diffusion coefficient (Eq. 5); s_c, characteristic shear rate for shear thinning (Eqs. 2b and 5); and b, shear thinning exponent (Eqs. 2b and 6).

†M1, The cytoplasm is Newtonian with weak membrane–cytoplasmic coupling and no cortical dissipation; M2, the cytoplasm is Newtonian with strong membrane–cytoplasmic coupling and no cortical dissipation; M3, the cytoplasm is shear thinning with weak membrane–cytoplasmic coupling and no cortical dissipation; M4, the cytoplasm is shear thinning with strong membrane–cytoplasmic coupling and no cortical dissipation; M5, the cytoplasm is Newtonian with strong membrane–cytoplasmic coupling and cortical dissipation; M6, the cytoplasm is shear thinning with strong membrane–cytoplasmic coupling and cortical dissipation.

gressively worsened as the aspiration pressure was increased. The more detailed temporal dynamics related to the various phases of neutrophil aspiration were also poorly represented by M1 (nevertheless, the model did at least predict something resembling the initial and final jumps and some sort of linear middle phase).

One possible explanation for the poor performance of M1 relates to the treatment of membrane diffusion. Accordingly, we next consider what happens when we take the opposite point of view (thus, in M2, we let $D_m = 0$ while all other parameters were kept the same as in M1, see Table 2). To illustrate the difference caused by this change, Fig. 4 shows some computations of the distribution of the excess area at the midpoint of aspiration. For M2 (Fig. 4 *a*), we see that the membrane is stretched on the part of the droplet surface that has entered the pipet and that it is wrinkled on the external part. Thus, there exists a sharp lateral gradient of wrinkles at the pipet opening (because of Eq. 5, there is also a sharp gradient of the surface tension). This gradient is generated during the early stages of aspiration because the flow near the axis of the pipet is faster than the flow at the corner. Eventually, this gradient acts to accelerate the surface flow at the rim and, thus, prevent a complete rupture of the membrane inside the pipet. In contrast, M1 has a lot of surface diffusion and, therefore, predicts that the distribution of membrane is almost uniform both inside and outside the pipet (Fig. 4 *b*). Notice, however, that, despite uniformity in space, the value of ρ is still a function of time because the total projected surface area of the mesh was increasing as aspiration progressed. Therefore, the hypothesis of a very large D_m is sufficient to guarantee that the plasma membrane remains intact at all points on the droplet surface without the need for a large tangential gradient of surface stress.

The results of computations based on M2 can be seen by referring to the appropriate theoretical curves in Fig. 3 (labeled *2*). A direct comparison with the corresponding predictions of M1 demonstrated that changing the diffusive transport of ρ had very little overall effect on the time scale of aspiration (a decrease on the order of 10–20%). Thus, in the final analysis, M1 and M2 were equally incompetent to account for the way in which the general time scale of aspiration depends on pressure and on pipet radius. We conclude that models without surface viscosity and with simple Newtonian treatments of the cytoplasmic viscosity can fit a limited amount of data by appropriate adjustments of the free parameters. However, such models cannot explain the dynamics of neutrophil aspiration if one considers data collected with different pipets and a range of different pressures. Overall, such models have no real predictive capability and failed to satisfy our stated utilitarian conditions for validity. As a side note, the cause of this poor performance was not related to assumptions about membrane diffusion (or the lack thereof).

The effect of shear thinning

Two striking features of M1 and M2 are the gross underestimation of the average rate of aspiration at high pressure and the growth of this error as the applied pressure was increased. The basic problem with M1 and M2 is that they predict a linear relationship between $\dot{L}_{p50}$ and ΔP, but, in actuality, the relationship is linear only at low pressures, and, as the pressure is increased, the relationship between $\dot{L}_p$ and ΔP seems to go like a power law with an exponent greater than one. These results should not be surprising because they are completely in agreement with the observations originally that led Tsai and coworkers to propose their shear thinning model of the neutrophil cytoplasm (Tsai et al., 1993). Accordingly, we next consider a new model, M3, in which values of s_c and b were chosen to fit the observed pressure dependence of $\dot{L}_{p50}$ in our five narrow pipet experiments. All other parameters (including μ_0) were the same as in M1 (see Table 2).

Comparison of M1 and M3 shows (see Fig. 3) that the introduction of shear thinning does produce a marked improvement in some aspects of model performance. In particular, with M3 there is good agreement in the observed time scale of aspiration between M3 and the data over the entire range of pressures in the narrow pipet experiments. However, in absolute terms, M3 still grossly and systematically underestimates the rate of aspiration in the wide pipet (Fig. 3, *f–h*). So, introducing shear thinning helps explain the nonlinear relationship between $\dot{L}_p$ and ΔP and thus yields an improved simulation of the effects of pressure on

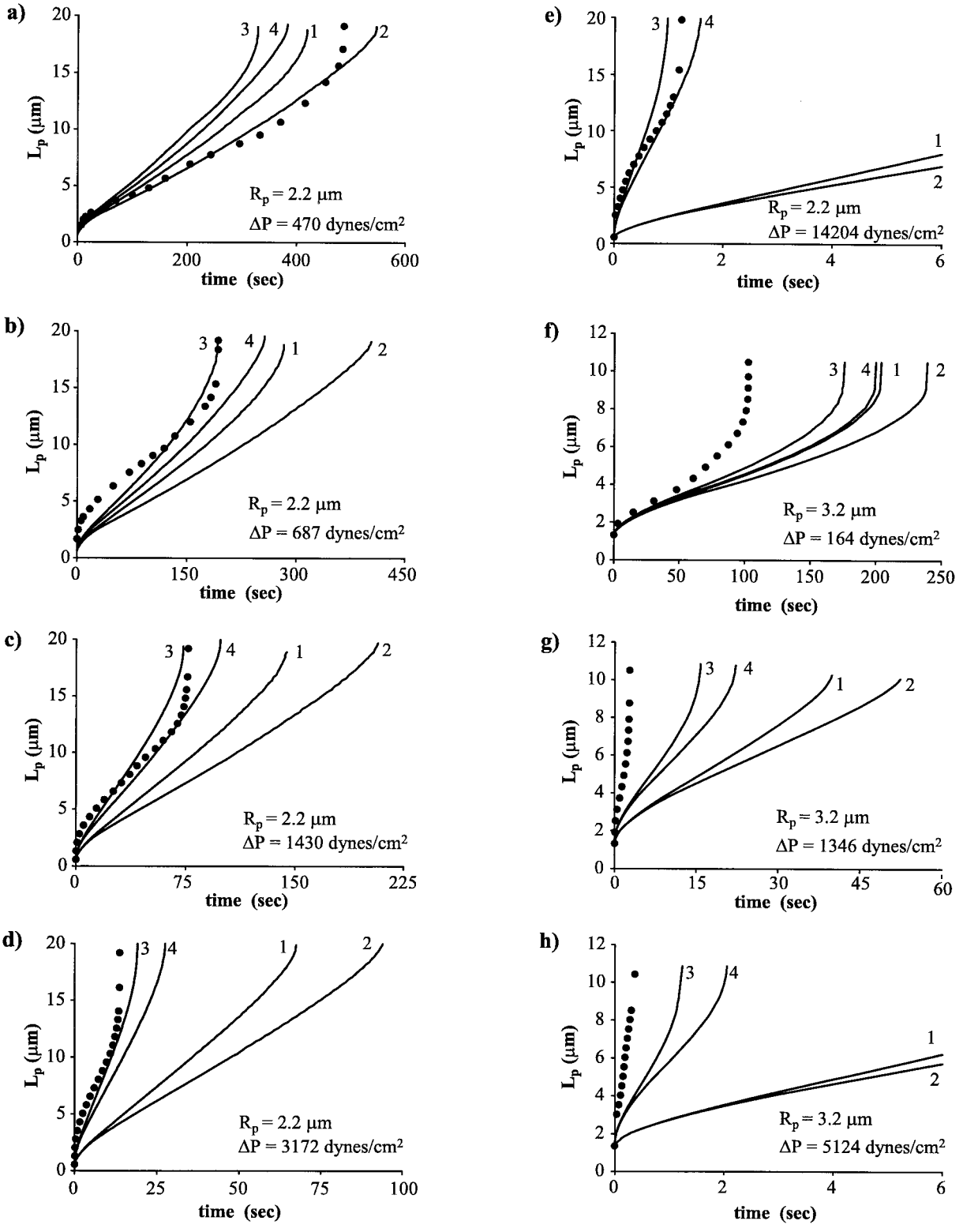

FIGURE 3 L_p versus time for various values of R_p and ΔP as indicated. Data (*circles*) represent combined results of all cells aspirated under each condition. Corresponding computational results (*solid lines*) are also indicated for the first four models of Table 2 (note labeling of curves, *1* for M1, *2* for M2, etc.). M1, has Newtonian cytoplasm with weak coupling to the plasma membrane, M2 has Newtonian cytoplasm with strong coupling to the plasma membrane, M3 has shear thinning cytoplasm with weak coupling, and M4 has a shear thinning cytoplasm with strong coupling. In all cases, the model parameters are as indicated in Table 2.

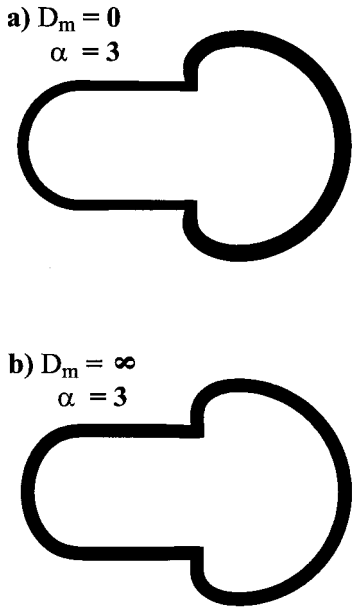

FIGURE 4 Effect of diffusive transport on the excess area distribution. The computed magnitude of ρ on various parts of the domain boundary is indicated as in a histogram, by the thickness of the outline. The computational parameters correspond to models M3 and M4 of Table 2 under conditions of Exp. 4 (R_p = 2.2 μm and ΔP = 3172 dynes/cm^2). Thus all parameters are identical, except that, in (*a*) $D_m = 0$ (strong membrane–cytoplasmic coupling) and, in (*b*) $D_m = \infty$ (free-slip between the membrane and cytoplasm). As can be seen, in the latter case, the distribution of excess area is uniform over the entire surface, whereas, in the former case, there is a sharp gradient of ρ near the entrance of the pipet.

the rate of aspiration at a given pipet diameter. Nevertheless, M3 still lacked any meaningful capacity to predict the effects of pipet radius on the average rate of aspiration. In addition, M3 was no better than M1 when it came to explaining the subtle temporal dynamics associated with the initial and final stages of aspiration.

Because M3 used the assumption of very fast membrane diffusion, it seemed possible to improve performance by changing this aspect of the model. Accordingly, we considered a new model (M4) with identical parameters as M3 except that $D_m = 0$ (see Table 2). Unfortunately, the computations in Fig. 3 indicate that there was no meaningful difference between the predictions of M3 and M4. As with the prior comparison of M1 and M2, this simply served to reconfirm that whether the plasma membrane could slip with respect to the cytoplasm is a rather minor factor in influencing the performance of these aspiration models.

The effect of surface viscosity

In the four models discussed above, the common factor is that energy dissipation only occurs in the bulk cytoplasm. With the inclusion of shear thinning, these models had some success at simulating the effects of pressure on the average rate of aspiration, but they were markedly deficient at simulating the effects of pipet diameter. This is troubling because capillary diameters vary significantly in different organs, and a model that fails to capture the consequences of this fact can have little physiological relevance. Similar anomalous effects of pipet radius on aspiration were originally observed by Evans and Yeung (1989), who suggested that these might be explained by the existence of a viscous resistance to dilation of the cell cortex. Mathematically, this means that the isotropic part of the total surface stress at any location on the boundary can be given by the sum of the usual *static* tension (γ) and a so-called *viscous* tension ($\eta\nabla_s \cdot \mathbf{v}$),

$$\gamma_{total} = \gamma + \eta\nabla_s \cdot \mathbf{v}. \quad (7)$$

The new coefficient, η, is the dilatational surface viscosity introduced previously (see Eq. 6).

The inclusion of viscous tension leads to an additional mode of energy dissipation, which scales like $\eta\dot{A}^2/A$. In contrast, we have shown previously (Drury and Dembo, 1999) that the dissipation due to shear viscosity of the bulk cytoplasm scales like $(2/\pi)\mu\dot{Q}^2(1/R_p^3 - 1/R_{max}^3)$. Letting $A \approx 4\pi R_c^2$, $\dot{A} \approx 2\dot{Q}(1/R_p - 1/R_{max})$ and assuming that η and μ have the same shear rate dependency, we then obtain the following order-of-magnitude estimate for the surface-to-interior dissipation ratio,

$$\varphi = \frac{\pi\eta\dot{A}^2/A}{2\mu\dot{Q}^2(R_p^{-3} - R_{max}^{-3})} \approx \frac{R_p\eta_0}{2R_c^2\mu_0}\frac{[1 - R_p/R_{max}]^2}{1 - (R_p/R_{max})^3}. \quad (8)$$

Note that neither ΔP nor any time derivatives appear on the right of this expression. This means that adding surface dissipation does not effect the basic underlying relationship between $\dot{L}_{p50}$ and ΔP so that, $\dot{L}_{p50}$ will still be linear in ΔP unless there is shear thinning. In contrast, Eq. 8 indicates that changing the pipet radius from 2.2 to 3.2 μm will lower φ by about one order of magnitude. This implies that the relative ease of aspiration in a wide versus narrow pipet will be greatly increased when surface dissipation is the dominant mechanism of resistance. Eq. 8 also indicates that, if surface dissipation is dominant, than the ease of aspiration will increase rapidly as aspiration proceeds, because R_{max} approaches R_p. This means that a model with surface dissipation predicts greater acceleration in $\dot{L}_p$ during the final stages of aspiration.

Consider the implications of Eq. 8 for the case of M4. As shown in Fig. 3, this model gave a good prediction of $\dot{L}_{p50}$ in Exp. 1 (low pressure, narrow pipet) but made a gross underestimate in the case of Exp. 6 (low pressure, wide pipet). According to Eq. 8, if we increase η_0 while simultaneously decreasing μ_0, then it should be possible to arrive at a situation where the good agreement in the narrow pipet experiment is maintained but where the aspiration into the wide pipet would be faster (thereby correcting the deficiency of M4). We tested this idea numerically, and, as

expected, several combinations of μ_0 and η_0 provided much improved agreement with both experiments 1 and 6. Models M5 and M6 in Table 2 represent cases in which the ratio η_0/μ_0 is at the upper limit of plausibility. In M5, both the surface and bulk viscosities are Newtonian, and in M6 they are shear thinning.

A comparison of M5 and M6 against our full data set is shown in Fig. 5. These results demonstrate that including cortical dissipation corrects the major problem of M4 (i.e., the overall poor performance in the wide pipet). Furthermore, if shear thinning is also included (M6) then this improvement is not purchased at the expense of a significantly decreased ability to simulate the effects of pressure. If shear thinning is not included (M5), then, even though the model has surface viscosity, it cannot explain the nonlinear effects of pressure on the rate of aspiration. The overall conclusion is that a droplet model with both cortical dissipation and shear thinning comes quite close to simulating the observed dependence of the aspiration time scale on both pipet radius and pressure. Droplet models that lacked either of these features have failed quite badly thus far. In general, one could doubtless obtain better overall agreement between theory and experiment by more extensive fitting procedures or by using different choices of shear thinning parameters for the surface viscosity. However, this would not change the basic qualitative conclusion as outlined.

As expected from Eq. 8, models with surface dissipation (M5 and M6) predict a large acceleration in the rate of droplet entry during the final moments of the aspiration process. As a result, the aspiration curves computed with M5 and M6 come quite close to explaining the final jump phase of aspiration. This is a very satisfying development because the final jump has previously been a pervasive and mysterious characteristic of neutrophil aspiration. As noted previously, droplet models without surface viscosity do a very poor job of simulating the final jump. Unfortunately, M6 still failed to adequately simulate the amplitude and speed of the initial jump. Thus, whatever causes this phenomenon seems to be independent of the factors causing the final jump (see Discussion).

A further unexpected benefit of including surface viscosity concerned the geometry of the cell near the end of aspiration. As shown in Fig. 6, at high pressures, models without surface dissipation (Fig. 6, *b–f*) flatten against the outer surface of the pipet, and, in some cases, a reentrant jet is formed. In the case of M6 (Fig. 6 *f*), however, the external surface of the cell remained quite round during the entire aspiration process, even at the highest pressures. This occurred because the dynamic surface tension scales with the aspiration rate so that the tension is sufficient to keep the cell close to a shape of minimum area even when the pressure was high. Surface viscosity also changes the dynamics of surface area creation and fluid entry into the pipet. Instead of new surface being created just inside the opening of the pipet (as seen in the models without surface viscosity), area is created more or less uniformly over the entire boundary (both inside and outside the pipet). The fact that models M1–M4 (Fig. 6, *6–e*) predict flattening against the exterior of the pipet leads to increased dissipation, which, in turn, seems to be the ultimate reason that these models fail to predict the observed increase in $\dot{L}_p$ during the final stages of aspiration.

DISCUSSION

By considering and testing a series of models of gradually increasing complexity, we have arrived at a certain construction (specifically, M6) capable of capturing the basic dependency of aspiration rate on pipet diameter and pressure for the cells of a single donor. In addition, this model is able to explain the observed round external geometry of cells being aspirated at high pressure and also the general amplitude and timing of the final acceleration of aspiration. Shear thinning of the cytoplasm and cortical dissipation were the key attributes that enable these desirable features.

According to our results, shear thinning in both the surface viscosity and the interior viscosity is crucial to understanding the pressure dependence of aspiration. In addition to the present results, one other group also found support for the reality of shear thinning in the neutrophil (Tsai et al., 1993). These workers reported a value of $b = 0.5$, which is what we obtain also. In another case, Needham and Hochmuth (1990) determined effective viscosities of cells from several different donors at both high and low aspiration pressures. In some donors, these authors did find shear thinning in the amount we would expect, but, in other donors, they detected none at all (see Table I of Needham and Hochmuth, 1990). Other evidence favoring the idea that the cytoplasm is some type of shear thinning fluid has come from rheological studies of purified microfilament and microtubule solutions (Zaner and Stossel, 1982; Buxbaum et al., 1987; Sato et al., 1988; Janmey, 1991; Xu et al., 1998). These studies indicated that, for the simple and controlled flow conditions of a cone and plate viscometer, the viscosity of these cytoskeletal polymers decreases according to a power law over a very wide range of shear rates. Of course the actual cytoplasm of living cells is much more complicated than these simple and well-defined model systems.

An explanation of the donor-to-donor differences observed by Needham and Hochmuth may lie in the internal cytoskeletal dynamics. For example, the inverse of the critical shear rate ($1/s_c \approx 20$ s) can be interpreted as a measure of the time constant for homeostatic repair of mechanical damage to the neutrophil cytoskeleton. Coincidentally, the value of 20 s is very close to the reported time constant for F-actin turnover in neutrophil lysates (Cano et al., 1991). This indicates that the repair of mechanical damage caused during aspiration occurs as part of a general homeostatic cycle in which the entire cytoskeleton of the neutrophil is continuously removed and regenerated. In this

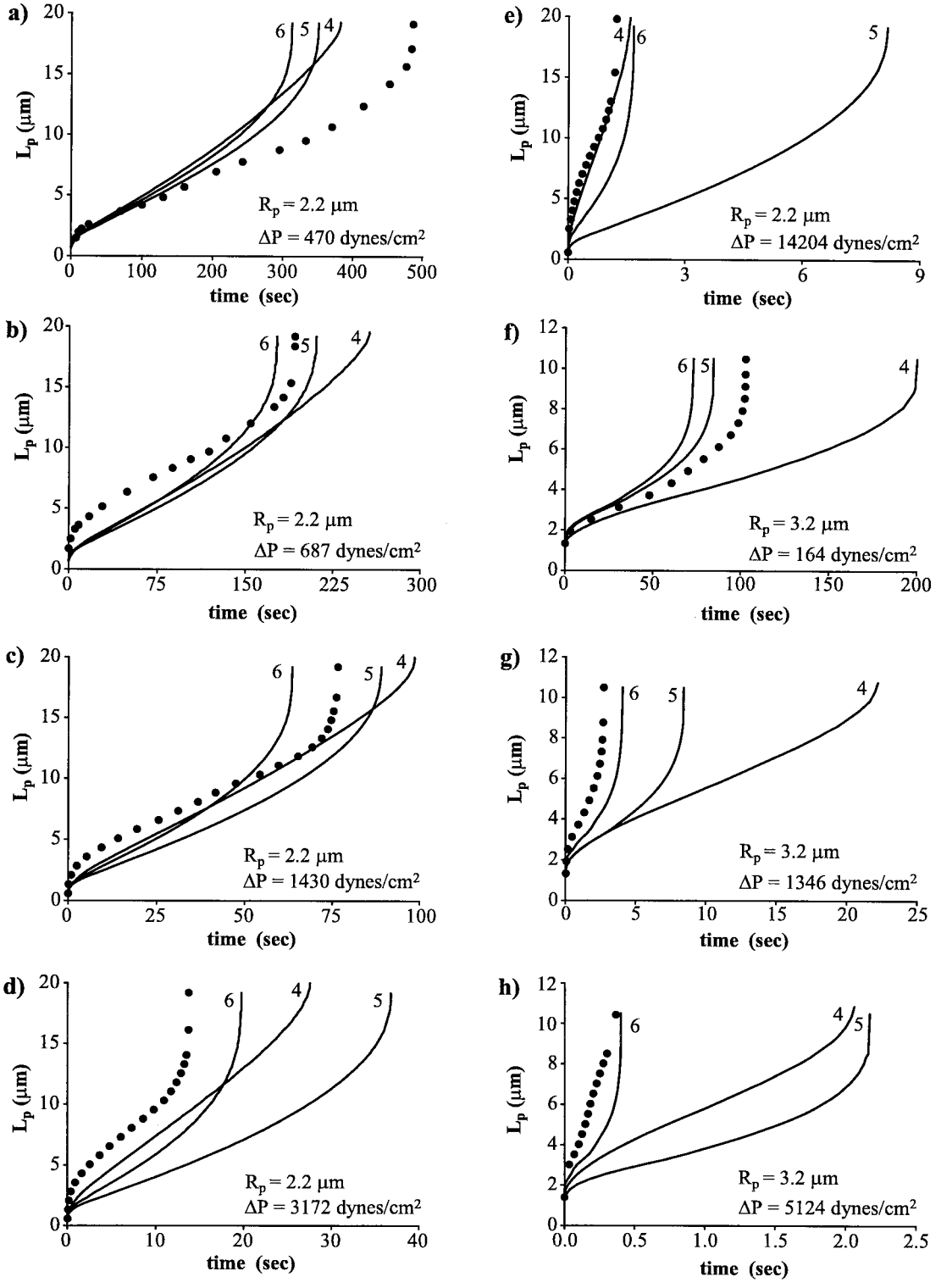

FIGURE 5 Effect of surface viscosity on model performance. Experimental data in the various panels (*circles*) are the same as in Fig. 3. Solid curves show the results of corresponding computations with Models 5 and 6 of Table 2. These models both include high surface viscosity in the context of either Newtonian cytoplasm (M5), or shear thinning cytoplasm (M6). For easy comparison with our prior results, we also reproduce the curves for one of the models without surface viscosity (M4).

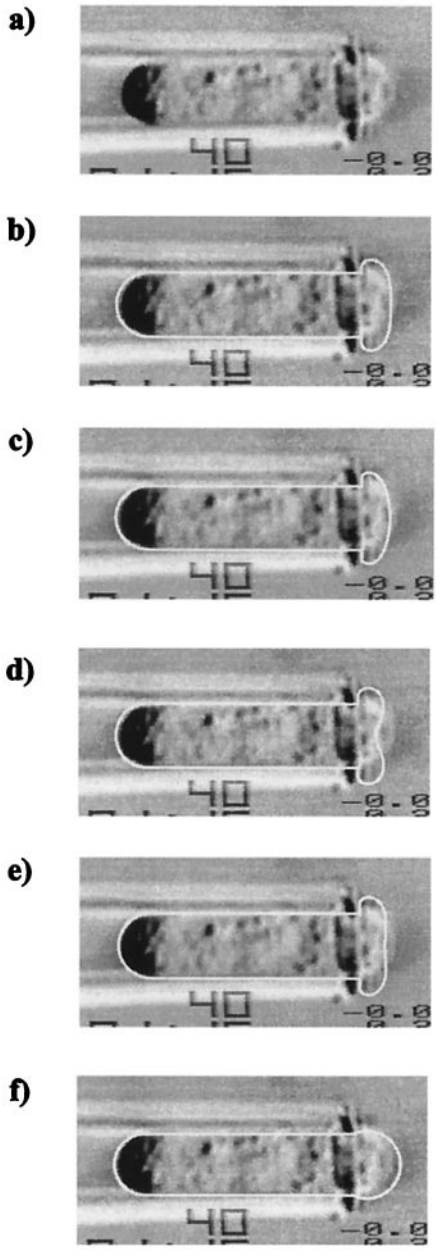

FIGURE 6 Comparison of experiment and theoretical predictions regarding the geometry of neutrophil near the completion of aspiration. Conditions correspond to those of Exp. 4 (R_p = 2.2 μm and ΔP = 3172 dynes/cm^2). (*a*), Only the video image of a typical neutrophil from this experiment. (*b*) The shape predicted with model M1 (Newtonian cytoplasm, infinite membrane diffusion, no surface viscosity) is superimposed over the image. Note that, in the calculation, the exterior portion of the boundary is extensively flattened against the pipet, whereas the actual data indicate that the exterior portion of the cell has a very round contour. Other models in which surface viscosity is neglected also invariably predict very flattened shapes, grossly inconsistent with the data, except at the lowest aspiration pressures. This is evident from panels (*c*), (*d*), and (*e*) that show calculations with M2, M3, and M4, respectively. In stark contrast, panel (*f*) shows the prediction of model M6, which includes high surface viscosity and shear thinning cytoplasm. Clearly, if significant surface viscosity is included, then one can get a much improved agreement between theory and experiment.

case, if aspiration were slow compared to this ongoing turnover, then naturally, there would be little mechanical degradation of the normal structure; and the coefficients of surface viscosity and cytoplasmic shear would be maintained at the constant values, η_0 and μ_0. If this picture is correct, then variations in the speed of the turnover cycle could explain the donor-to-donor differences observed by Needham and Hochmuth. For example if, in some people, the speed of the cycle were increased by 10-fold, then shear thinning would be very difficult to detect.

Many labs have reported values of the viscosity of the neutrophil cytoplasm for different pressure ranges and pipet sizes (e.g., Needham and Hochmuth, 1990; Hochmuth and Needham, 1990; Trans-Son-Tay et al., 1991; Hochmuth et al., 1993; Tsai et al., 1993). These various groups also used different constitutive laws and data-processing approaches in their attempts to extract this parameter from the raw aspiration data. Nevertheless, in each case, the final answer indicated a viscosity on the order of 1000 poise, which is close to our result. In addition, the consensus among these estimates is that the apparent viscosity is lower if the cells are aspirated by large-diameter pipets. This anomalous dependence of apparent viscosity on pipet diameter is strong indirect evidence in favor of cortical dissipation. Aside from this indirect evidence, the main prior support for the concept of cortical dissipation was presented by Evans and Yeung (1989). Unfortunately, the value of the apparent surface viscosity derived by these authors is much smaller than the value we have now obtained ($\eta_0 \sim 0.1$ versus $\sim$100 poise $\cdot$ cm). We have no ready explanation for this discrepancy, but the outcome is that our present results ascribe a much greater importance to surface viscosity than previously indicated. For example, it is easy to estimate (see Eq. 8) that, with the parameters of M6 in a 2.2-μm pipet, 10 times more energy will be dissipated by the cell cortex then by the bulk cytoplasm. Thus, if M6 is correct, it means that the cell cortex is the dominant factor in neutrophil mechanics; it not only generates the static tension but is also the main locus for viscous resistance to deformation.

In sum, M6, which includes both shear thinning of the cytoplasm and cortical dissipation, has considerable explanatory power. As yet, this is the only model of neutrophil mechanics that can explain this much of the available data. Nevertheless, it is a minimal model, and its most palpable failure concerns the mechanism of the initial deceleration phase of aspiration (initial jump). Undoubtedly, M6 will need to be generalized if this mystery is to be resolved.

One approach that has been suggested to explain the initial phase of aspiration envisions a shell of low viscosity material between the membrane and the high viscosity core (Evans and Yeung, 1989; Dong et. al., 1991; Dong and Skalak, 1992). Obviously, the outer zone of low resistance could facilitate initial aspiration, but the effect would rapidly diminish as the more viscous material in the core of the cell began to enter the pipet. We do not favor this model

because it would predict enhanced flattening of the cell against the pipet and because it seems to be incompatible with the idea that most resistance comes from the cortex. Another possibility is to generalize M6 by introducing a Maxwell model for the viscous cortical stress. Incorporation of shear thinning would ensure the proper dependence of the rate of aspiration on both the pipet size and aspiration pressure. We are currently in the process of working out the details of these various approaches to see if they can really help explain the initial jump.

APPENDIX A DERIVATION OF EQ. 3

Our purpose here is to clarify the physical meaning of the "diffusion term" appearing on the right of Eq. 3 of the main text (i.e., the transport equation for the excess area density). We start by imagining that the plasma membrane of the neutrophil is able to slip laterally over the cortical cytoplasm, but that it is unable to separate in the normal direction. This means that, in general, the membrane moves according to a distinct velocity field $\mathbf{u} \neq \mathbf{v}$ but that, at least, the normal component of velocity is the same as for the underlying cytoplasm, $\mathbf{u} \cdot \mathbf{n} = \mathbf{v} \cdot \mathbf{n}$. To find the independent components of $\mathbf{u}$, we need to consider the microscopic balance of forces acting in the tangent plane,

$$\mathbf{t} \cdot [f(\mathbf{v} - \mathbf{u}) + \nabla_s \gamma_m] = 0. \quad \text{(A1)}$$

Here, $\mathbf{t}$ is any unit tangent vector, and f is the coefficient of sliding friction between the membrane and the interior. Also, the coefficient γ_m represents the component of the total surface tension, which acts purely within the plasma membrane, (the total surface tension γ is obtained by combining this so-called membrane tension with the tension in other layers of the cortex). We now note that the surface gradient of a scalar lies in the tangent plane and that the membrane tension is some function of ρ. We can thus rearrange Eq. A1 to obtain

$$\mathbf{u} = [\mathbf{n} \cdot \mathbf{v}]\mathbf{n} + \left[\mathbf{t} \cdot \left[\mathbf{v} + \frac{\nabla_s \gamma}{f}\right]\right]\mathbf{t} = \mathbf{v} + \frac{\partial_\rho \gamma_m}{f} \nabla_s \rho. \quad \text{(A2)}$$

This has to be combined with the continuity equation governing transport of ρ,

$$\partial_t \rho + \mathbf{u} \cdot \nabla_s \rho = -\rho \nabla_s \cdot \mathbf{u}, \quad \text{(A3)}$$

to obtain a formulation in which the unknown membrane velocity $\mathbf{u}$ has been eliminated,

$$\partial_t \rho = -\nabla_s \cdot \rho \mathbf{v} - \nabla_s \cdot \left(\frac{\rho \partial_\rho \gamma_m}{f} \nabla_s \rho\right). \quad \text{(A4)}$$

Introducing the material derivative, $d_t \equiv \partial_t + \mathbf{v} \cdot \nabla_s$, and defining a membrane diffusion coefficient, $D_m \equiv -\rho \partial_\rho \gamma_m / f$, then yields the desired result,

$$d_t \rho = \nabla_s \cdot (D_m \nabla_s \rho) - \rho \nabla_s \cdot \mathbf{v}. \quad \text{(A5)}$$

One should note that the quantity D_m is positive as long as the membrane tension is a decreasing function of ρ. One should also note that the transport process described by this coefficient formally resembles a diffusion term but that the underlying physics is purely deterministic and has nothing to do with Brownian motion.

This work was supported by a Whitaker Special Opportunities Award in Cellular Mechanics.

The Authors wish to thank the Boston University Scientific Computing Center for use of their facilities. Special thanks to Dr. Evan Evans and his lab group at the University of British Columbia for their advice and assistance with the aspiration experiments.

REFERENCES

Albarran, B., H. P. Ting-Beall, and R. M. Hochmuth. 2000. Effect of surface area change on cortical tension in passive neutrophils. *Biophys. J.* 78:187A.

Aris, R. 1989. Vectors, Tensors and the Basic Equations of Fluid Mechanics. Dover Publications, New York.

Bird, R. B., W. E. Stewart, and E. N. Lightfoot. 1960. Transport Phenomena. John Wiley & Sons, New York.

Buxbaum, R. E., T. Dennerll, S. Weiss, and S. R. Heidemann. 1987. F-actin and microtubule suspension as indeterminate fluids. *Science.* 235:1511–1514.

Cano, M. L., D. A. Lauffenburger, and S. H. Zigmond. 1991. Kinetic analysis of F-actin depolymerization in polymorphonuclear leukocyte lysates indicates that chemoattractant stimulation increases actin filament number without altering the filament length distribution. *J. Cell Biol.* 115:677–687.

Dembo, M. 1994a. On free boundary problems and amoeboid motion. *In* Biomechanics of Active Movement and Division of Cells. N. Akkas, editor. NATO Advanced Study Institute Series, Springer-Verlag, Berlin. 231–283.

Dembo, M. 1994b. Solution of a continuum representation of the cytoplasmic mechanics by a finite element method. Los Alamos Unclassified Report No. 94-3454.

Dong, C., and R. Skalak. 1992. Leukocyte deformability: finite element modeling of large viscoelastic deformation. *J. Theoret. Biol.* 158: 173–193.

Dong, C., R. Skalak, K.-L. P. Sung, G. W. Schmid-Schönbein, and S. Chien. 1988. Passive deformation analysis of human leukocytes. *J. Biomech. Eng.* 110:27–36.

Dong, C., R. Skalak, and K.-L. P. Sung. 1991. Cytoplasmic rheology of passive neutrophils. *Biorheology.* 28:557–567.

Drury, J. L., and M. Dembo. 1999. Hydrodynamics of micropipet aspiration. *Biophys. J.* 76:110–128.

Evans, E., and B. Kukan. 1984. Passive material behavior of granulocytes based on large deformation and recovery after deformation tests. *Blood.* 64:1028–1035.

Evans, E., and A. Yeung. 1989. Apparent viscosity and cortical tension of blood granulocytes determined by micropipet aspiration. *Biophys. J.* 50:151–160.

He, X., and M. Dembo. 1997. On the mechanics of the first cleavage division of the sea urchin egg. *Exp. Cell Res.* 233:252–273.

Hochmuth, R. M., and D. Needham. 1990. The viscosity of neutrophils and their transit times through small pores. *Biorheology.* 27:817–828.

Hochmuth, R. M., H. P. Ting-Beall, B. B. Beaty, D. Needham, and R. Tran-Son-Tay. 1993. Viscosity of passive human neutrophils undergoing small deformations. *Biophys. J.* 64:1596–1601.

Hoffman, R., and L. Gross. 1975. The modulation contrast microscope. *Nature.* 254:586–588.

Janmey, P. A. 1991. Mechanical properties of cytoskeletal polymers. *Curr. Opin. Cell Biol.* 2:4–11.

Lipowsky, H. H., D. Riedel, and G. S. Shi. 1991. In vivo mechanical properties of leukocytes during adhesion to venular endothelium. *Biorheology.* 28:53–64.

Needham, D., and R. M. Hochmuth. 1990. Rapid flow of passive neutrophils into a 4 μm pipet and measurements of cytoplasmic viscosity. *J. Biomech. Eng.* 112:269–276.

Needham, D., and R. M. Hochmuth. 1992. A sensitive measure of surface stress in the resting neutrophil. *Biophys. J.* 61:1664–1670.

Sato, M., W. H. Schwartz, S. C. Selden, and T. D. Pollard. 1988. Mechanical properties of brain tubulin and microtubules. *J. Cell Biol.* 106: 1205–1211.

Schmid-Schönbein, G. W., Y. Y. Shih, and S. Chien. 1980. Morphometry of human leukocytes. *Blood.* 56:866–875.

Schmid-Schönbein, G. W., K.-L. P. Sung, H. Tözeren, R. Skalak, and S. Chien. 1981. Passive mechanical properties of human leukocytes. *Biophys. J.* 36:243–256.

Shao, J.-Y., and R. M. Hochmuth. 1997. The resistance to flow of individual human neutrophils in glass capillary tubes with diameters between 4.65 and 7.75 μm. *Microcirculation.* 4:61–74.

Sung, K.-L. P., C. Dong, G. W. Schmid-Schönbein. S. Chien, and R. Skalak. 1988. Leukocyte relaxation properties. *Biophys. J.* 53:331–336.

Ting-Beall, H. P., D. Needham, and R. M. Hochmuth. 1993. Volume and osmotic properties of human neutrophils. *Blood.* 81:2774–2780.

Tran-Son-Tay, R., D. Needham, A. Yeung, and R. M. Hochmuth. 1991. Time-dependent recovery of passive neutrophils after large deformation. *Biophys. J.* 60:856–866.

Tsai, M. A., R. S. Frank, and R. E. Waugh. 1993. Passive mechanical behavior of human neutrophils: power-law fluid. *Biophys. J.* 65: 2078–2088.

Xu, J., W. H. Schwarz, J. A. Käs, T. P. Stossel, P. A. Janmey, and T. D. Pollard. 1998. Mechanical properties of actin filament networks depend on preparation, polymerizations conditions, and storage of actin monomers. *Biophys. J.* 74:2731–2740.

Yeung, A., and E. Evans. 1989. Cortical shell-liquid core model for passive flow of liquid-like spherical cells into micropipets. *Biophys. J.* 56: 139–149.

Zaner, K. S., and T. P. Stossel. 1982. Some perspectives on the viscosity of actin filaments. *J. Cell Biol.* 93:987–991.